

The effect of the underlying mathematical model on particle size estimates by the laser diffraction method of needle-like particles

Okpeafoh S. Agimelen^{a,*}, Jan Sefcik^a, Anthony J. Mulholland^{b,*}

^a*EPSRC Centre for Innovative Manufacturing in Continuous Manufacturing and Crystallisation, Department of Chemical and Process Engineering, University of Strathclyde, James Weir Building, 75 Montrose Street, Glasgow, G1 1XJ, United Kingdom.*

^b*Department of Mathematics and Statistics, University of Strathclyde, Livingstone Tower, 26 Richmond Street, Glasgow G1 1XH, United Kingdom.*

Abstract

Many industrial processes for the production of particulate products rely on the accurate measurement of the sizes of these particles during the production process. One particle sizing technique which is implemented in commercial instruments due to its wide use in the manufacturing (of particulate products) industry is the laser diffraction method. The estimation of particle sizes by this method requires the solution of an inverse problem using a suitable model which incorporates the size, shape and optical properties of the particles. However, the commercial instruments which implement this laser diffraction method typically employ a model designed for spherical particles to solve this inverse problem even though a significant number of materials occur as elongated particles in industrial processes.

As the inverse problem is ill-posed, then the use of a spherical model could lead to very misleading results. In this work, we demonstrate that the use of this spherical model for the estimation of sizes of these elongated particles could lead to over estimation of the proportion of the small particles in the population. This effect could lead to an under estimation of the mean particle size by as much as a factor of 50%.

Keywords: Particle size distribution, Particle shape, Laser diffraction.

1. Introduction

Particle characterisation is one of the core tasks performed in the particle analysis community [1]. This activity involves the identification of the distribution of particle sizes¹ in a given powder sample which had been prepared by a suitable crystallisation technique. In some cases, the particle size distribution (PSD) of the crystals in a slurry

*Corresponding authors

Email addresses: okpeafoh.agimelen@strath.ac.uk (Okpeafoh S. Agimelen), anthony.mulholland@strath.ac.uk (Anthony J. Mulholland)

¹The particle size in this work is taken to be the diameter of a sphere for the case of spherical particles. Here, needle-like particles will be represented by infinite cylinders. In that case, the particle

could be directly estimated before the powder is produced. To achieve this task of PSD estimation (whether in situ or off-line), various techniques or equipment are utilised [1].

The laser diffraction method has become very popular in the particle analysis community, and for this reason different manufacturers have developed instruments which implement this technique [2]. This laser diffraction method involves the collection of scattered light from a dilute slurry of particles by an array of detectors placed at different spatial locations so that they cover a certain span of angles θ . Since the intensity of scattered light at (different angular positions) by each particle is a function of the size (and shape) of the particle, then the size distribution of the original population of particles that produced a particular scattering intensity (the intensity of scattered light as a function of angular position) can be inferred from the scattering intensity. However, as there is typically a distribution of particle sizes in a slurry, then the intensity pattern measured by the detectors will be a convolution of the intensity patterns from all the particles (of different sizes) in the slurry.

The estimation of the PSD from the measured scattering intensity involves solving an inverse problem using a suitable forward model. This forward model describes the scattering intensity to be expected from a particle of a given shape and size. This inversion process is typically implemented in the software of commercial laser diffraction instruments. However, these instruments typically implement (for solving the inverse problem) the Mie scattering model [3] for spherical particles regardless of the shape of the particles in the slurry. This has led to some inexplicable peaks and discrepancies [4, 5] in the PSD estimates with these instruments when the shape of the particles in the slurry deviate significantly from spherical. This could give misleading information regarding the distribution of particles sizes in a slurry. The consequences could be severe in applications where the process is very sensitive to the distribution of particle sizes. This is particularly important in the pharmaceutical industry where many of the active pharmaceutical ingredients are crystalline with needle-like shapes.

In this paper, we demonstrate some of the effects of using a spherical model to solve the inverse problem associated with laser diffraction for needle-like particles. Rather than using experimental data we deliberately use simulated data so that all of the observed effects are solely due to the inversion process and not other compounding issues that experimental data exhibit. We use three simulated monodispersed population of needle-like particles corresponding to particles in size ranges typically encountered in crystallisation processes, we show where the effect of solving the inverse problem with a spherical model could be more severe and where the effect is less severe.

2. Method

In this work, the scattering intensity for needle-like particles will be simulated using the scattering theory for infinitely long cylinders [3]. The cylindrical shape is a good

size will be the diameter of the circular cross section of the cylinder. The length of the cylinders cannot be specified as the cylinders have infinite length.

approximation for needle-like particles which are thin and elongated like cylinders. For example the cases of cellobiose octaacetate (COA), benzoic acid (BA) and metformin (MFM) are shown in Figs. 1(a), 1(b) and 1(c) respectively. Even though the cylindrical model is developed for infinitely long cylinders², the theory is applicable for needle-like particles whose lengths are four times or more [7] their radii (assuming a circular cross section for each particle). This requirement is easily satisfied by typical needle-like particles as seen in Fig. 1.

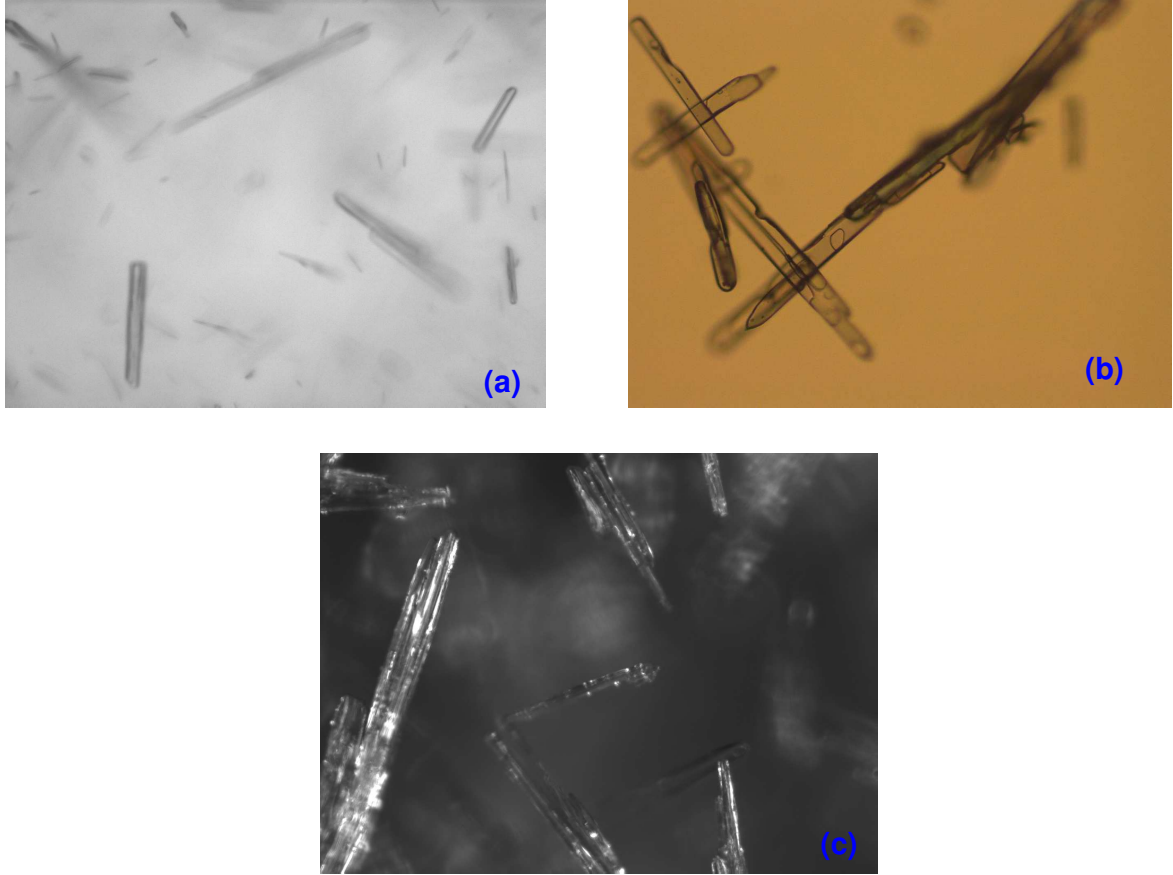


Figure 1: Sample images for typical needle-like particles for (a) COA, (b) BA and (c) MM crystals.

Simulated scattering intensity (as opposed to using experimentally measured scattering intensity for needle-like particles) will be used here so as to isolate the effect that the spherical model assumption has on the estimated PSD as experimental data would contain noise³ which would complicate the analysis. This is because inverse problems of this nature are not well posed [8, 9] such that the estimated PSD is heavily influenced

²A cylinder whose length is much larger than its diameter [6].

³The noise would be from various effects such as background noise from the measuring instrument, agglomeration of particles, distribution of the shape of the particles under consideration and so on.

by the noise from experiments. The simulated scattering intensity will not be contaminated by experimental noise, hence the effect can be ignored in the analysis. However, there will still be noise in the system due to errors from using the spherical model. The approach that will be adopted in this work will be to compute the scattering intensity for needle-like particles (of specified optical properties) using the model for infinitely long cylinders, and then solve the inverse problem using the Mie model for spherical particles. Since the PSD of the needle-like particles will be specified, then the estimated PSD obtained using the spherical model can be compared with the known PSD to check the level of agreement with the known PSD.

3. Calculating scattering intensity

Consider a detector system (sketched in Fig. 2(a)) in which a monochromatic light with wave vector \mathbf{k}_i is incident on a particle of arbitrary size and shape. The scattered light with wave vector \mathbf{k}_s is then collected at different angles θ to the direction of propagation of the incident light by an array of detectors as depicted in Fig. 2. Both the incident and scattered light have components parallel and perpendicular to the scattering plane (the plane containing the incident and scattered light) [3]. The scattering wave vector \mathbf{q} is the difference between the incident and scattered wave vectors as sketched in Fig. 2(b). The magnitude of the scattering wave vector is a function of the scattering angle θ , and it is given by [10]

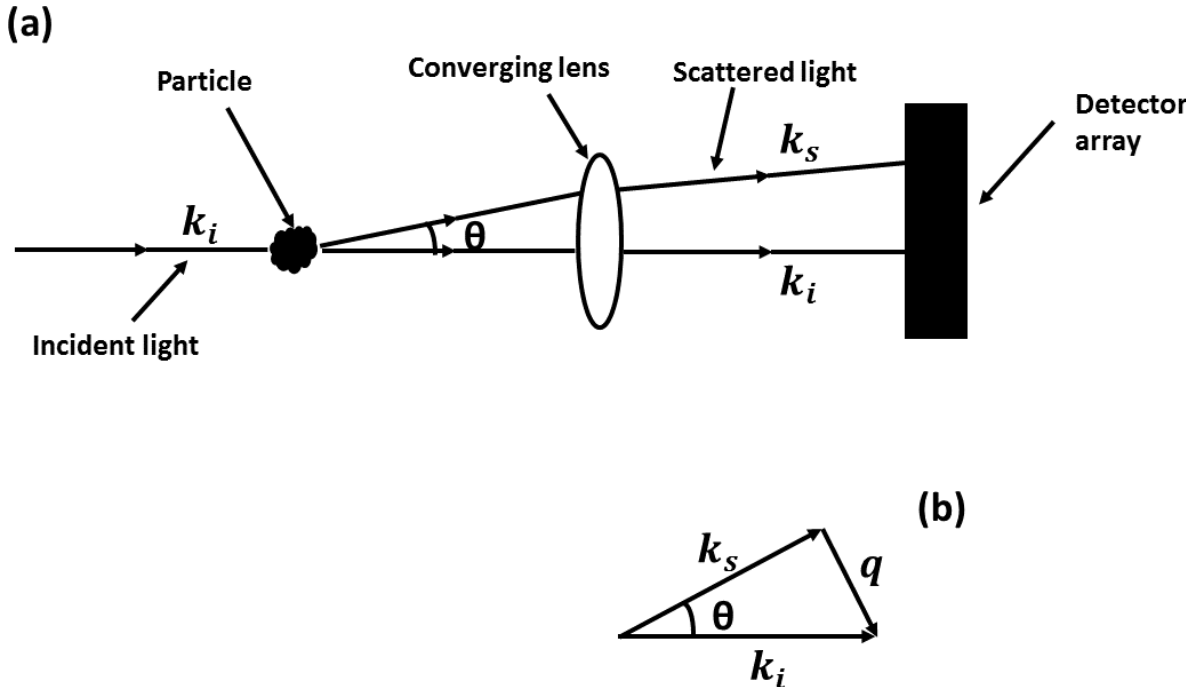


Figure 2: (a) Schematic of the setup of typical laser diffraction instruments. (b) Illustration of the scattering wave vector.

$$q = \frac{4\pi}{\lambda} \sin(\theta/2), \quad (1)$$

where λ is the wavelength of the incident light.

The general information concerning the intensity and state of polarisation of both the incident and scattered light is contained in the Stokes parameters I, Q, U, V [3, 11]. The Stokes parameter I is the light flux or intensity. The Stokes parameters Q and U describe the state of linear polarisation and V describes the state of circular polarisation. The Stokes parameters of the incident light are related to those of the scattered light by means of the scattering matrix or phase matrix \mathbf{Z} as [3, 11]

$$\begin{pmatrix} I_s \\ Q_s \\ U_s \\ V_s \end{pmatrix} = \frac{1}{k^2 r^2} \begin{pmatrix} Z_{11} & Z_{12} & Z_{13} & Z_{14} \\ Z_{21} & Z_{22} & Z_{23} & Z_{24} \\ Z_{31} & Z_{32} & Z_{33} & Z_{34} \\ Z_{41} & Z_{42} & Z_{43} & Z_{44} \end{pmatrix} \begin{pmatrix} I_i \\ Q_i \\ U_i \\ V_i \end{pmatrix}, \quad (2)$$

where $k = 2\pi/\lambda$ is the wave number and r is distance in the radial direction. The Stokes parameters of the scattered light are indicated by the subscript s , while those of the incident wave are indicated by the subscript i in Eq. (2). The elements $Z_{ij}, ij = 1, 2, 3, 4$ of the phase matrix \mathbf{Z} are related to the elements of the amplitude matrix \mathbf{S} . The amplitude matrix relates the incident electric field \mathbf{E}_i to the scattered electric field \mathbf{E}_s as [3, 11]

$$\begin{pmatrix} E_{\parallel s} \\ E_{\perp s} \end{pmatrix} = \frac{e^{ik(r-z)}}{-ikr} \begin{pmatrix} S_2 & S_3 \\ S_4 & S_1 \end{pmatrix} \begin{pmatrix} E_{\parallel i} \\ E_{\perp i} \end{pmatrix}, \quad (3)$$

where the incident light is taken to propagate in the z direction. The elements $S_i, i = 1, 2, 3, 4$ of the amplitude matrix are functions of the scattering angle θ , the size of the particle D and the refractive index N_R of the particle.

Most commercial laser diffraction instruments only measure the intensity of scattered light from an incident unpolarised light. Hence it is assumed in this work that there is no polarisation of the scattered light so that the Stokes parameters $Q = U = V = 0$. Thus Eq. (2) reduces to

$$I_s = \frac{Z_{11}}{k^2 r^2} I_i, \quad (4)$$

where Z_{11} is given by [3]

$$Z_{11} = \frac{1}{2} (|S_1|^2 + |S_2|^2 + |S_3|^2 + |S_4|^2). \quad (5)$$

In a population of particles of different sizes and shapes, the phase matrix for the population will be the sum of the phase matrices of the individual particles in the population. Then the phase matrix for the population is given as [3, 11]

$$\mathbf{Z} = \sum_{k=1}^N \mathbf{Z}_k, \quad (6)$$

where \mathcal{N} is the number of particles in the population. The sum in Eq. (6) holds provided that the particles are randomly positioned and oriented, and that the particles are sufficiently spaced such that there is no multiple scattering. Hence the intensity of scattered light from the population of particles will be given as

$$I = \frac{I_0}{k^2 r^2} \sum_{k=1}^{\mathcal{N}} Z_{11,k}, \quad (7)$$

where I_0 and I are the intensities of the incident and scattered light respectively and $Z_{11,k}$ is the contribution to the Z_{11} component of the phase matrix from particle k . The conditions required for Eq. (6) to hold are easily met in commercial laser diffraction instruments, hence the conditions will be assumed to apply in this work.

Here, the polydispersed population of particles shall be assumed to consist of particles of the same shape and refractive index but different sizes. The distribution of particle sizes is characterised by a probability density function $n(D)$ such that $n(D)dD$ is the probability of finding particles with diameters between D and $D + dD$. If the diameters of the particles are discretised and grouped into N geometrically spaced size classes such that the characteristic diameter of particles whose diameters lie between D_i and D_{i+1} ($i = 1, 2, \dots, N$) is given by $\bar{D}_i = \sqrt{D_i D_{i+1}}$, then a discretised particle size distribution (PSD) $X(\bar{D}_i)$ can be defined such that $X(\bar{D}_i)$ is the number of particles whose diameters lie between D_i and D_{i+1} .

Then the number of particles \mathcal{N}_i with characteristic diameter \bar{D}_i is given by $\mathcal{N}_i = X(\bar{D}_i)$. Then Eq. (7) can be rewritten as

$$I(\theta_j) = \frac{I_0}{k^2 r^2} \sum_{i=1}^N \mathcal{N}_i Z_{11}(\theta_j, \bar{D}_i) = \frac{I_0}{k^2 r^2} \sum_{i=1}^N Z_{11}(\theta_j, \bar{D}_i) X(\bar{D}_i), \quad (8)$$

where the scattering angle θ has been discretised into $j = 1, 2, \dots, M$ angular positions and $Z_{11}(\theta_j, \bar{D}_i)$ is the averaged phase matrix component for particles whose sizes lie between D_i and D_{i+1} . Since the magnitude of the scattering wave vector q is a function of angle (as defined in Eq. (1)), then the scattering intensity and component Z_{11} of the phase matrix in Eq. (8) can be rewritten as functions of q (discretised) as

$$I(q_j) = \frac{I_0}{k^2 r^2} \sum_{i=1}^N Z_{11}(q_j, \bar{D}_i) X(\bar{D}_i). \quad (9)$$

Writing $I(q_j)$ as I_j , $Z_{11}(q_j, \bar{D}_i)$ as $\tilde{Z}_{j,i}$ and $X(\bar{D}_i)$ as X_i , then Eq. (9) can be written as a matrix equation as

$$I_j = \mathbf{I} = \frac{I_0}{k^2 r^2} \sum_{i=1}^N \tilde{Z}_{j,i} X_i = \frac{I_0}{k^2 r^2} \tilde{\mathbf{Z}} \mathbf{X}. \quad (10)$$

The scaling factor in Eq. (10) can be removed if the scattering intensity is rescaled by the scattering intensity I_1 measured at an angular position close to zero. That is,

the zero q limit of the scattering intensity. The choice of I_1 for rescaling the scattering intensity is reasonable since the quantity Z_{11} assumes a flat profile at the zero q limit for particles of different shapes and sizes and refractive indices [3]. If the first detector in the array of detectors (sketched in Fig. 1) is placed at an angular position sufficiently close to zero, then the scattering intensity at the zero q limit for the particles in the N size classes can be constructed from the first row of matrix $\tilde{\mathbf{Z}}$ as

$$I_1 = \frac{I_0}{k^2 r^2} \sum_{i=1}^N \tilde{Z}_{1,i} X_i. \quad (11)$$

Then the rescaled scattering intensity \tilde{I}_j can be constructed as

$$\tilde{I}_j = \frac{I_j}{I_1} = \frac{\sum_{i=1}^N \tilde{Z}_{j,i} X_i}{\sum_{i=1}^N \tilde{Z}_{1,i} X_i}. \quad (12)$$

The rescaled scattering intensity in Eq. (12) is the form in which the scattering intensity data is reported in typical commercial laser diffraction instruments. Hence this form of the scattering intensity will be used in subsequent analysis in this work.

3.1. Population of spherical particles

The components $S_3 = S_4 = 0$ in the amplitude matrix defined in Eq. (3) in the case of spherical particles [3]. The components S_1 and S_2 are defined as [3]

$$S_1 = \sum_n \frac{2n+1}{n(n+1)} (a_n \pi_n + b_n \tau_n) \quad (13a)$$

$$S_2 = \sum_n \frac{2n+1}{n(n+1)} (a_n \tau_n + b_n \pi_n), \quad (13b)$$

where the quantities π_n and τ_n are functions of the scattering angle θ . They can be obtained by the following recurrence formulas [3]

$$\pi_n = \frac{2n-1}{n-1} \mu \pi_{n-1} - \frac{n}{n-1} \pi_{n-2} \quad (14a)$$

$$\tau_n = n \mu \pi_n - (n+1) \pi_{n-1}, \quad (14b)$$

where $\mu = \cos(\theta)$, $\pi_0 = 0$ and $\pi_1 = 1$. The series in Eqs. (13) and (14) are truncated after n_c terms; the value of which is related to the size of the particle [3]. The scattering coefficients a_n and b_n are functions of the particle size and refractive index. They are obtained by solving the Maxwell equations for a spherical particle with appropriate boundary conditions⁴. Using Eq. (5), then the Z_{11} component of the phase matrix can be calculated and subsequently the rescaled scattering intensity of the population can be calculated using Eq. (12).

⁴See [3] for details of the calculations of the scattering coefficients. The numerical calculations of these scattering coefficients (for spherical particles) has been implemented in various programming languages. The Matlab implementation by [12] is used in this work.

3.2. Population of needle-like particles

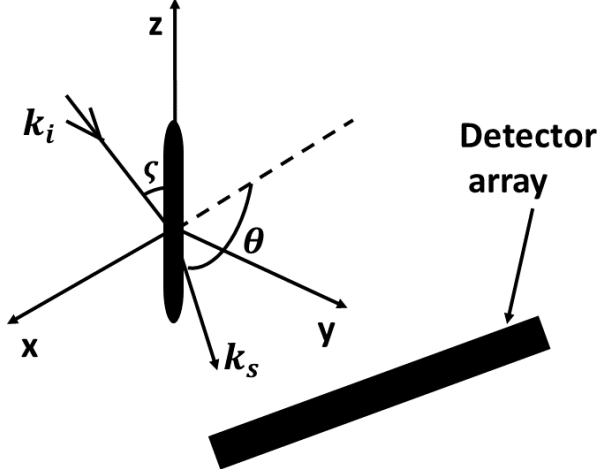


Figure 3: A schematic for light scattering by an infinitely long cylinder.

As discussed in section 2, the scattering intensity of needle-like particles will be approximated with that for infinitely long cylinders. The sketch of such an infinitely long cylinder is shown in Fig. 3. The axis of the cylinder lies along the z -axis. The incident light (with wave vector \mathbf{k}_i) which is contained in the $x - z$ plane makes an angle ζ with the cylinder axis, while the scattered light (with wave vector \mathbf{k}_s) is contained in the $x - y$ plane and makes an angle θ with the negative x -axis. The scattered light is measured in the $x - y$ plane by an array of detectors as shown in Fig. 3. The scattering plane contains the cylinder axis and scattered light [3].

The amplitude matrix relates the incident electric field \mathbf{E}_i to the scattered electric field \mathbf{E}_s as [3]

$$\begin{pmatrix} E_{\parallel s} \\ E_{\perp s} \end{pmatrix} = e^{i3\pi/4} \sqrt{\frac{2}{\pi kr \sin(\zeta)}} e^{ik(r \sin(\zeta) - z \cos(\zeta))} \begin{pmatrix} T_1 & -T_3 \\ T_3 & T_2 \end{pmatrix} \begin{pmatrix} E_{\parallel i} \\ E_{\perp i} \end{pmatrix}, \quad (15)$$

The quantities $T_i, i = 1, 2, 3$ in Eq. (15) correspond to the quantities $S_i, i = 1, 2, 3, 4$ in Eq. (3) for the general case. The quantities $T_i, i = 1, 2, 3$ are given as [3]

$$T_1 = \hat{b}_{0I} + 2 \sum_{n=1}^{\infty} \hat{b}_{nI} \cos(n\theta) \quad (16a)$$

$$T_2 = \hat{a}_{0II} + 2 \sum_{n=1}^{\infty} \hat{a}_{nII} \cos(n\theta) \quad (16b)$$

$$T_3 = -2i \sum_{n=1}^{\infty} \hat{a}_{nI} \sin(n\theta). \quad (16c)$$

The scattering coefficients $\hat{b}_{0I}, \hat{b}_{nI}, \hat{a}_{0II}, \hat{a}_{nII}, \hat{a}_{nI}$ (similar to the case of a_n and b_n in Eq. (13)) are functions of particle size (the diameter of the infinitely long cylinder) and

refractive index. They are obtained by solving the Maxwell equations for the cylindrical geometry with appropriate boundary conditions⁵.

Using the components $T_i, i = 1, 2, 3$ of the amplitude matrix for the infinitely long cylinder, then the Z_{11} component of the phase matrix can be calculated as

$$Z_{11} = \frac{1}{2} (|T_1|^2 + |T_2|^2 + 2|T_3|^2). \quad (17)$$

Subsequently the rescaled scattering intensity in Eq. (12) can be calculated for the infinitely long cylinders that are used to represent needle-like particles in this work.

4. Forward and inverse problem

In a slurry of particles of different sizes, the scattering intensity measured $\tilde{\mathbf{I}}^*$ with a suitable instrument will be a convolution of the scattering intensities of the individual particles in the slurry and the PSD \mathbf{X} as discussed in section 3. If the PSD \mathbf{X} of the particles in the slurry is given, then the scattering intensity of the population can be calculated by solving the forward problem in Eq. (12). This calculated scattering intensity $\tilde{\mathbf{I}}$ can then be compared with the measured scattering intensity.

In reality the PSD \mathbf{X} of the particles in a slurry will not be known. Instead the situation will be to estimate the PSD corresponding to a measured scattering intensity. This situation will involve solving an inverse problem. As mentioned earlier, the purpose of this work is to examine the effect of the model employed in solving the inverse problem on the solutions obtained. To achieve this objective, then the experimentally measured scattering intensity $\tilde{\mathbf{I}}^*$ will be simulated with the model for infinitely long cylinders by means of Eq. (17). Then a different scattering intensity $\tilde{\mathbf{I}}$ will be calculated using the Mie model for spherical particles. This calculated scattering intensity $\tilde{\mathbf{I}}$ will then be used to solve the inverse problem for a given $\tilde{\mathbf{I}}^*$.

In this work, the inversion to obtain the PSD \mathbf{X} will be carried out by solving the weighted least square problem given as

$$\min f = \sum_{j=1}^M w_j \left[\tilde{I}_j^* - \tilde{I}_j \right]^2, \quad (18)$$

which is an unconstrained optimisation problem [13]. The weight function w_j is given as

$$w_j = \frac{1}{1 + |C_1|\tilde{I}_j + |C_2|\tilde{I}_j^2}, \quad (19)$$

where the quantities C_1 and C_2 are optimisation parameters with initial values $C_1 = C_2 = 0$. The weighting function in the objective function in Eq. (18) is necessary as

⁵See [3] for a detailed discussion of the calculation of these coefficients. The numerical computations of these coefficients were carried out in Matlab in this work.

the values of the scattering intensity cover several orders of magnitude over the entire q range of interest. A similar weighting function was employed in [14] for the calculation of intensity for anti-Stokes Raman scattering but with fixed values of C_1 and C_2 .

4.1. Number and volume based PSD

The PSD defined in Eq. (8) which is calculated by solving the least square problem in Eq. (18) is number based. The number based PSD X_i is defined as an exponential function of the parameter γ_i as

$$X_i = e^{\gamma_i}, i = 1, 2, \dots, N. \quad (20)$$

Then the optimisation problem given in Eq. (18) is solved by searching for γ_i (using the Levenberg-Marquardt algorithm as implemented in Matlab) which minimises the objective function f given in Eq. (18). As the Levenberg-Marquardt method is gradient based and the objective function in Eq. (18) contains local minima, then a multi-start strategy [15] is used to search for a global minimum. This involves using different random starting solutions for γ_i , then the solution for which the L_2 norm given as

$$\|\tilde{\mathbf{I}}^* - \tilde{\mathbf{I}}\|_2 = \sqrt{\sum_{j=1}^M \left[\tilde{I}_j^* - \tilde{I}_j \right]^2} \quad (21)$$

is minimum is then chosen as the optimum. Subsequently the number based PSD X_i in Eq. (20) is calculated from this optimum solution for γ_i .

However, as commercial laser diffraction instruments typically report a volume based PSD, then it is necessary to calculate a corresponding volume based PSD. This can be achieved as follows. Consider the scattering intensity \bar{I}_j (obtained in a manner similar to the case of I_j in Eq. (10)) given as

$$\bar{I}_j = \alpha \sum_{i=1}^N \tilde{Z}_{ji} \hat{X}_i, \quad (22)$$

where

$$\alpha = \frac{I_0}{k^2 r^2} \quad (23)$$

and

$$\hat{X}_i = \frac{X_i}{\sum_{i=1}^N X_i}. \quad (24)$$

The scattering intensity \bar{I}_j is associated with the number based PSD X_i by means of Eq. (22). However, the scattering intensity \bar{I}_j can also be associated with the volume based PSD X_i^v (the total volume of particles of sizes between D_i and D_{i+1}) by writing

$$\bar{I}_j = \alpha \sum_{i=1}^N \bar{Z}_{ji} \bar{X}_i^v, \quad (25)$$

where

$$\bar{Z}_{ji} = \frac{\tilde{Z}_{ji}}{D_i^3}, \quad (26)$$

$$\bar{X}_i^v = \hat{X}_i^v \sum_{i=1}^N \hat{X}_i D_i^3 \quad (27)$$

and

$$\hat{X}_i^v = \frac{\hat{X}_i D_i^3}{\sum_{i=1}^N \hat{X}_i D_i^3}. \quad (28)$$

Then the scattering intensity \bar{I} can be normalised to remove the scaling factor α (as in the case of Eq. (12)) as

$$\hat{I}_j = \frac{\sum_{i=1}^N \bar{Z}_{ji} \bar{X}_i^v}{\sum_{i=1}^N \bar{Z}_{1i} \bar{X}_i^v}. \quad (29)$$

Hence Eq. (29) becomes the forward problem for the volume based PSD⁶ similar to the case of Eq. (12) for the number based PSD.

The volume based PSD X_i^v can then be calculated by solving a weighted least square problem similar to the case given in Eq. (18). A similar approach has previously been implemented for different sensor data [8, 9].

The method of computing the volume based PSD X_i^v is carried out as follows. Obtain the number based PSD X_i whose corresponding scattering intensity \hat{I}_j gives the best fit to the scattering intensity \hat{I}_j^* of the needle-like particles as judged by the L_2 norm in Eq. (21). Then using this optimum number based PSD, construct the scattering intensity \bar{I}_j given in Eq. (22). Then normalise the scattering intensity \bar{I}_j to obtain the scattering intensity \hat{I}_j in Eq. (29) as $\hat{I}_j = \bar{I}_j / \bar{I}_1$, where \bar{I}_1 is the zero q limit of \bar{I}_j . This scattering intensity \hat{I}_j is associated with the volume based PSD X_i^v defined in Eq. (29). When \hat{I}_j is computed for needle-like particles, then it is written as \hat{I}_j^* .

To obtain the volume based PSD, search for values of the parameters γ_i^v for which the volume based PSD \bar{X}_i^v which is defined as

$$\bar{X}_i^v = e^{\gamma_i^v}, i = 1, 2, \dots, N \quad (30)$$

gives a scattering intensity (by means of the normalised matrix multiplication in Eq. (29)) \hat{I}_j which is closest to \hat{I}_j^* . The search for the parameters γ_i^v is done by solving a weighted least square problem similar to that in Eq. (18) given as

$$\min f_v = \sum_{j=1}^M w_j^v \left[\hat{I}_j^* - \hat{I}_j \right]^2, \quad (31)$$

⁶The association of the scattering intensity \bar{I}_j to the volume based PSD given in Eq. (25) can only be made for particles with defined volume, for example spherical particles. However, as the sizes of the infinitely long cylinders used in this work are monodispersed, then the number based PSDs will coincide with the corresponding volume based PSDs of the infinitely long cylinders even though the volume of an infinitely long cylinder is not defined.

where w_j^v is a weight function similar to the case of Eq. (19) for the number based PSD.

The optimisation problem in Eq. (31) is solved using the Levenberg-Marquardt algorithm as implemented in Matlab. Since the scattering intensity \bar{I}_j in Eq. (22) was constructed from a number based PSD obtained at the global minimum of the objective function f in Eq. (18), then an initial estimate X_i^{v0} of the volume based PSD which is close to the global minimum of the objective function f_v in Eq. (31) can be constructed by the method of truncated singular value decomposition (TSVD) [15] using the scattering intensity \hat{I}_j in Eq. (29). This initially estimated volume based PSD X^{v0} can then be used to obtain an initial starting solution for γ_i^v and passed on to the Levenberg-Marquardt algorithm to solve the optimisation problem in Eq. (31). The TSVD method can only be used to generate an initial estimate for γ_i^v as it predicts PSDs with negative values because of the ill-posed nature of the inverse problem. However, the formulation of the volume based PSD \bar{X}_i^v in Eq. (30) guarantees non-negative values.

Finally, the volume based PSD is normalised as

$$\hat{X}_i^v = \frac{\bar{X}_i^v}{\sum_i^N \bar{X}_i^v}. \quad (32)$$

4.2. Mean particle size

The mean size of the particles in a population can be represented by various metrics depending on the application [16]. The volume weighted mean diameter D_{43} is commonly reported by commercial laser diffraction instruments. The D_{43} value is defined as [16]

$$D_{43} = \frac{\sum_{i=1}^N X_i \bar{D}_i^4}{\sum_{i=1}^N X_i \bar{D}_i^3}, \quad (33)$$

which upon using the substitution $X_i^v = X_i v_i$ (where v_i is the volume of the spherical particle with diameter \bar{D}_i) becomes

$$D_{43} = \sum_{i=1}^N \hat{X}_i^v \bar{D}_i, \quad (34)$$

where

$$\hat{X}_i^v = \frac{X_i^v}{\sum_{i=1}^N X_i^v} \quad (35)$$

is the volume fraction of spherical particles of size \bar{D}_i . This D_{43} value will coincide with the size of spherical particles in a monodispersed population. Otherwise, it will give an estimate of the mean size of the spherical particles in a polydispersed population.

5. Results and Discussion

Needle-like particles in a slurry will experience different kinds of hydrodynamic conditions depending on the vessel type, the stirrer type and speed, restrictions to flow, the size and suspension density of particles and so on. Based on these different conditions, the particles may be able to perform completely random rotations or they could become aligned with the flow field. When the particles perform different random rotations, then the incoming monochromatic light will hit the needle-like particles at different angles to their axes. However, when the needle-like particles are aligned with the flow field, then the incoming monochromatic light will hit the particles within some restricted angles to their axes. This is because the flow cells typically used in the measurements have limited space for particle rotations, and the source of light illuminates the flow cell within some restricted angles depending on the design of the instrument [17]. Hence when the particles are aligned with the flow field (and hence the flow cell), then the incident angle of the incoming light to the particles will also be limited. Motivated by this, we consider the two special situations where the incoming light is normally incident to the axes of the particles on one hand and when the incoming light hits the particles at different angles to their axes on the other hand.

These two extremes will be examined in this work. When the particles are free to perform different random rotations, then the incident angle ζ (see Fig. 3) of the incoming monochromatic light will take all possible values from $\zeta \approx 0^\circ$ (grazing incidence) to $\zeta = 90^\circ$ (normal incidence). However, when the particles are aligned with the flow field, then the incoming monochromatic light will be normally incident on the particles and hence the incident angle ζ is fixed at 90° .

The refractive indices of materials typically encountered in pharmaceutical crystallisation processes are of order $N_r = 1.50$ with zero absorption. For example, the COA, BA and MM crystals shown in Fig. 1 have refractive indices of $N_r = 1.51, 1.50$ and 1.58 respectively. The three materials have poor solubility in methanol which has a refractive index $N_r = 1.33$. Hence the refractive index of $N_r = 1.50$ was used in the simulation of the scattering intensities of the needle-like particles (modelled as infinitely long cylinders), and the particles were assumed to be suspended in a medium with refractive index $N_r = 1.33$. For the inverse problem, the spherical particles were assumed to have the same refractive index of $N_r = 1.50$ and also suspended in a medium with a refractive index of $N_r = 1.33$. Hence any discrepancy between the scattering intensities from the needle-like particles and the spherical particles will only be due to the difference in shape and not the optical properties.

5.1. Case I: restricted rotations

The black diamonds in Fig. 4(a) show the scattering intensity from needle-like particles (simulated with the model for infinitely long cylinders⁷) with a monodispersed

⁷In this case, the scattering coefficients in Eq. (17) are computed at a single angle $\zeta = 90^\circ$ which are then used to calculate the scattering matrix components T_1, T_2 and T_3 to obtain the scattering

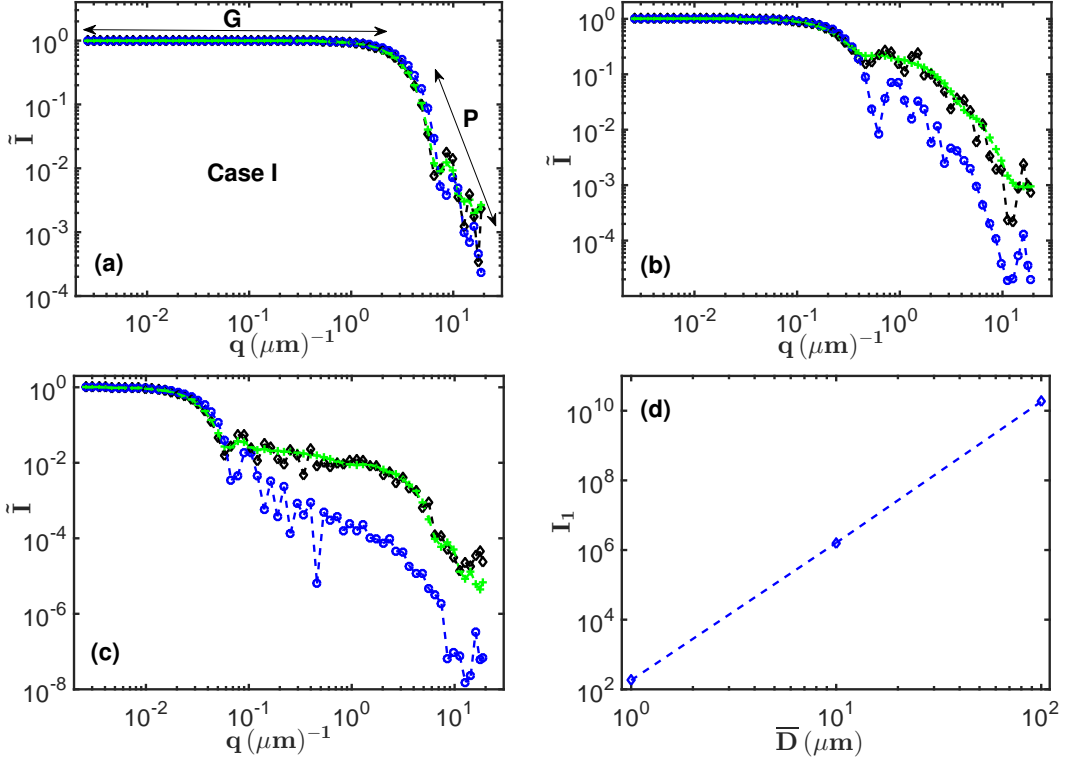


Figure 4: Black diamonds: scattering intensities for needle-like particles with monodispersed sizes of (a) $D = 1\mu\text{m}$, (b) $D = 10\mu\text{m}$ and (c) $D = 100\mu\text{m}$ for Case I. Green crosses: estimated scattering intensities (by solving the optimisation problem in Eq. (19)) using the spherical model corresponding to the scattering intensities from the needle-like particles in (a), (b) and (c). The blue circles in (a), (b) and (c) are the scattering intensities for spherical particles (by solving the forward problem in Eq. (12)) of monodispersed sizes of (a) $D = 1\mu\text{m}$, (b) $D = 10\mu\text{m}$ and (c) $D = 100\mu\text{m}$. (d) The zero q limits of the scattering intensities for spherical particles of the sizes shown.

distribution of particle size (diameter of circular cross section of the cylinders) of $D = 1\mu\text{m}$ as shown by the black diamonds in Fig. 5(a). The green crosses show the estimated scattering intensity by using the spherical model in solving the optimisation problem in Eq. (31). The estimated scattering intensity with the spherical model shows a good fit with the original scattering intensity for the needle-like particles. The corresponding estimated PSD with the spherical model is shown by the green crosses in Fig. 5(a). The estimated PSD obtained using the spherical model shows a peak at a particle size slightly larger than $D = 1\mu\text{m}$ as shown by the green crosses in Fig. 5(a). It also shows a peak at a particle size close to $0.2\mu\text{m}$. This can be understood by applying a simple scaling law analysis.

This scaling law approach predicts a scattering intensity which is independent of q [10] for $qR \lesssim 1$ (where R is the radius of the particle) after which it transits into the

intensity.

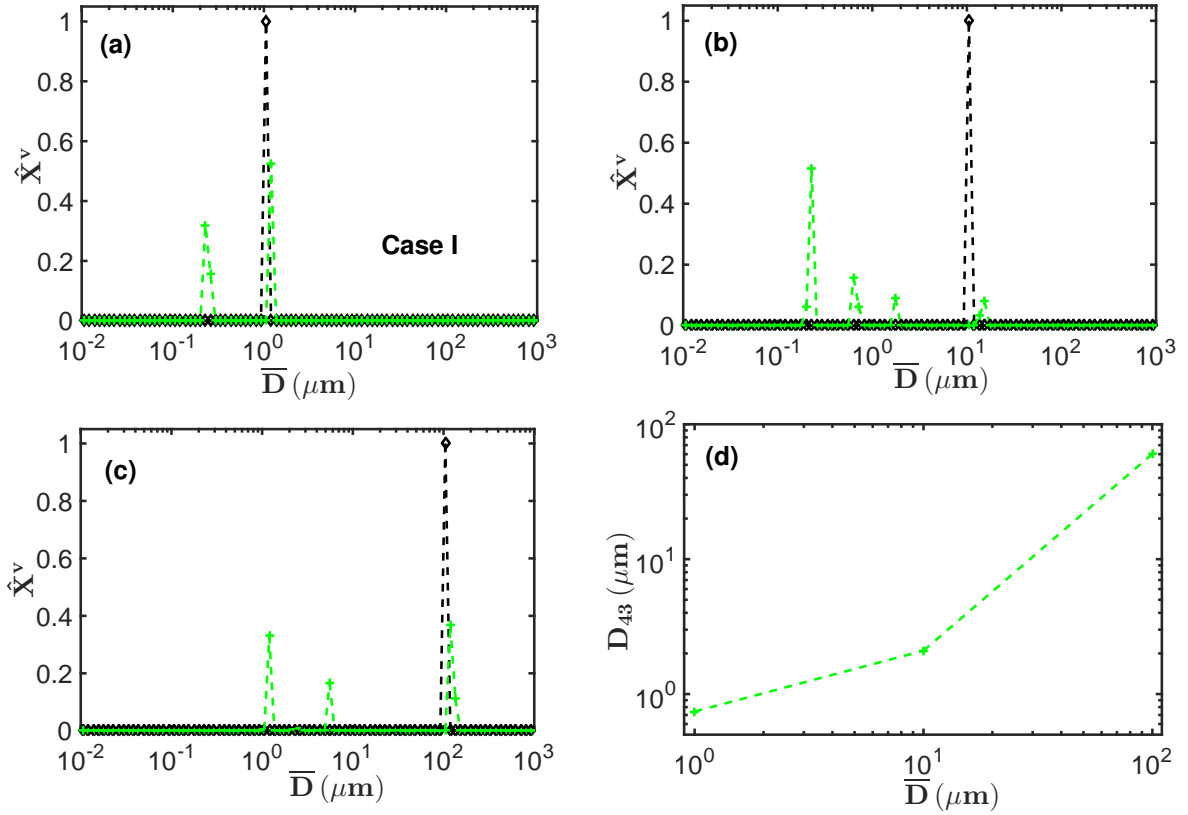


Figure 5: Black diamonds: monodispersed distribution of sizes for needle-like particles of sizes (a) $D = 1\mu\text{m}$, (b) $D = 10\mu\text{m}$ and (c) $D = 100\mu\text{m}$ for Case I. Green crosses: estimated PSD using the spherical model to solve the optimisation problem in Eq. (31) for the scattering intensities of the needle-like particles whose PSDs are shown by the black diamonds. (d) The D_{43} values estimated from the PSDs obtained with the spherical model.

power law regime where it decays with a q scaling depending on the type of particle [10]. This q independent regime or Guinier regime is indicated as G in Fig. 4(a) while the power law regime is indicated as P in the same Fig. The transition from the Guinier to the power law regime occurs at $qR \approx 1$.

The blue circles in Fig. 4(a) represent the scattering intensity for a spherical particle of diameter $1\mu\text{m}$. This scattering intensity has a slightly longer Guinier regime when compared with the scattering intensity of a needle-like particle (simulated with the model for infinitely long cylinders) with circular cross sectional diameter $1\mu\text{m}$. Hence in order for the spherical model to fit the Guinier regime of the needle-like particles, it overestimates the diameter of the needle-like particle⁸. This leads to the prediction of particles with sizes slightly larger than $1\mu\text{m}$ by the spherical model as shown by the green crosses in Fig. 5(a).

⁸Note that the Guinier regime of spherical particles become shorter (that is, the transition from the Guinier to the power law regime shifts to the left) as the size of the particle increases.

The power law regime of the scattering intensity for spherical particles slightly falls below that of the needle-like particles in the high q ($q \gtrsim 5\mu\text{m}$ in Fig. 4(a)) region. Hence the spherical model introduces particles of size $\bar{D} \approx 0.2\mu\text{m}$ and weights the fraction of these particles appropriately in order for it to fit the high q region of the power law regime of the needle-like particles. This is the reason for the peak at $\bar{D} \approx 0.2\mu\text{m}$ in Fig. 5(a) (green crosses) in the estimated PSD using the spherical model. This is because the smaller spherical particles have a slightly longer Guinier regime so that their introduction and appropriate weighting leads to a better fit of the power law regime (in the high q region) of the needle-like particles by the spherical model.

A similar situation holds for needle-like particles of sizes $\bar{D} = 10\mu\text{m}$ and $\bar{D} = 100\mu\text{m}$. The Guinier regime of the scattering intensities corresponding to needle-like particles of these sizes ($\bar{D} = 10\mu\text{m}$ and $\bar{D} = 100\mu\text{m}$) are slightly shorter (black diamonds in Figs. 4(b) and (c)) than the Guinier regime of monodispersed spherical particles of corresponding sizes (blue circles in Fig. 4(b) and (c)). Hence in order for the spherical model to fit the Guinier regime of the needle-like particles (green crosses in Figs. 4(b) and (c)), the spherical model predicts PSDs which contain peaks at locations slightly larger than $10\mu\text{m}$ and $100\mu\text{m}$ respectively as seen by the peaks in Figs. 5(b) and (c).

Furthermore, the PSDs predicted by the spherical model contains peaks at particles sizes $< 10\mu\text{m}$ (for the case of needle-like particles of size $\bar{D} = 10\mu\text{m}$) as seen by the green crosses in Fig. 5(b) and at particles sizes $< 100\mu\text{m}$ (for the case of needle-like particles of size $100\mu\text{m}$) as shown by the green crosses in Fig. 5(c). This is because the power law regime of the scattering intensities of spherical particles of sizes $\bar{D} = 10\mu\text{m}$ and $\bar{D} = 100\mu\text{m}$ (blue circles in Figs. 4(b) and (c) respectively) decays faster than the power law regime of the scattering intensities of needle-like particles with corresponding sizes (black diamonds in Figs. 4(b) and (c) respectively). This faster decay of the scattering intensities of the spherical particles leads to the introduction of smaller particles (than the actual sizes of the needle-like particles) by the spherical model in order for the spherical model to fit the power law regime of the needle-like particles.

The spherical model weights the peaks of the smaller particles appropriately in order to fit the power law regime of the needle-like particles. The volume fraction of the small particles introduced by the spherical model to fit the power law regime of the needle-like particles could be substantial as seen in the case of $\bar{D} = 10\mu\text{m}$ in Fig. 5(b). This is because the plateau value of the Guinier regime (the zero q limit of the scattering intensity defined as I_1 in Eq. (11)) varies by orders of magnitude for particles of different sizes as shown in Fig. 4(d).

Due to the introduction of smaller particles (than the sizes of the corresponding needle-like particles), the D_{43} values calculated with the estimated volume based PSDs from the spherical model are significantly smaller than the sizes of the needle-like particles as seen in Fig. 5(d). This shows that the spherical model will predict a mean particle size which is less than the true mean size of the needle-like particles when these needle-like particles are aligned with the flow and the incoming light is incident normally to the axes of the particles.

5.2. Case II: random rotations

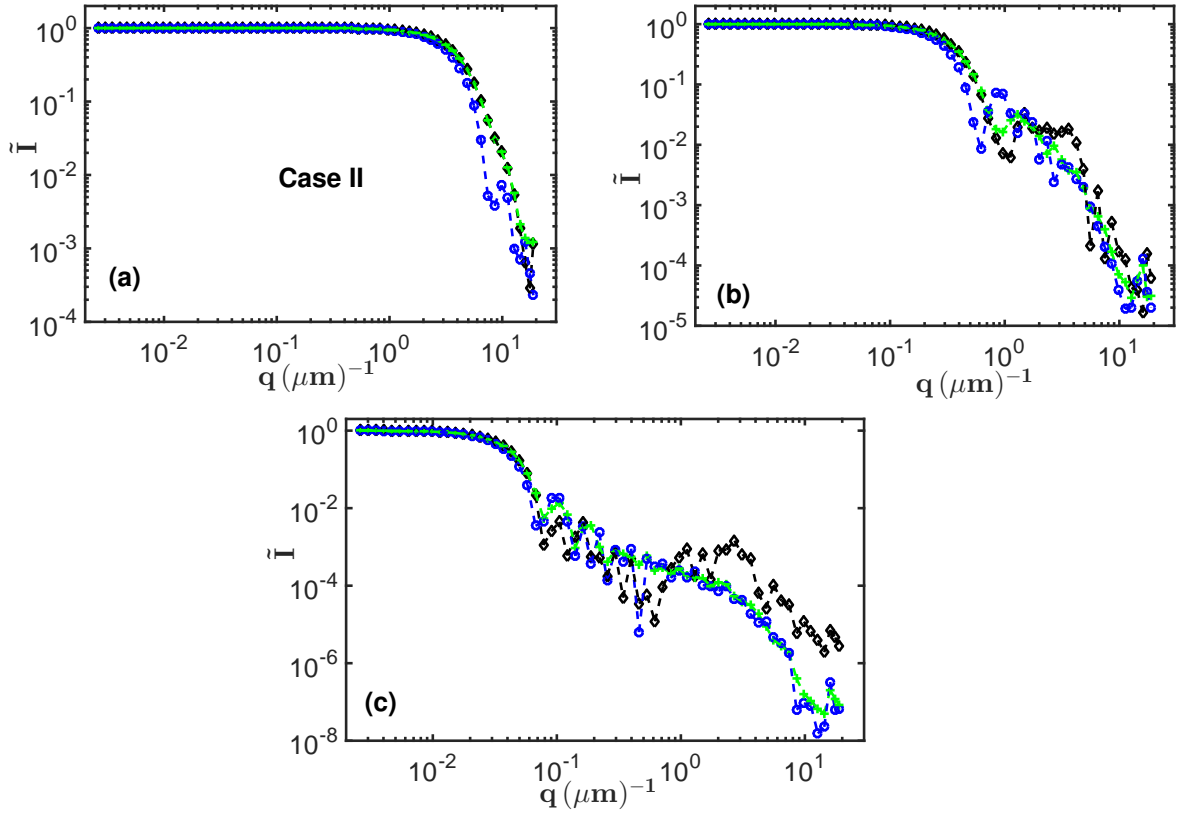


Figure 6: Similar to Figs. 4 (a), (b) and (c) but for Case II.

The other extreme where the needle-like particles are able to make random rotations is analysed in this section. As in Case I, the scattering intensity of the needle-like particles will be simulated⁹ with the model for infinitely long cylinders, while the inverse problem will be solved with the Mie model for spherical particles.

Unlike in Case I, the Guinier regime of the scattering intensity (blue circles in Fig. 6(a)) for spherical particles of size $\bar{D} = 1\mu\text{m}$ is slightly shorter than that of needle-like particles (black diamonds in Fig. 6(a)) of the same size. This leads the spherical model to predict the largest particle size to be less than $1\mu\text{m}$ (the size of the needle-like particles) as shown by the green crosses in Fig. 7(a). However, as the power law regime of the scattering intensity (blue circles in Fig. 6(a)) of the spherical particles of size $\bar{D} = 1\mu\text{m}$ decays faster than that (black diamonds in Fig. 6(a)) of needle-like particles, then the spherical model introduces smaller particles (as shown by the peaks in the

⁹In this case, the scattering coefficients in Eq. (17) are computed for values of $\zeta = 1^\circ, 2^\circ, \dots, 90^\circ$, and then averaged over ζ . The averaged scattering coefficients are then used to calculate the components T_1, T_2 and T_3 in order to compute the scattering intensity.

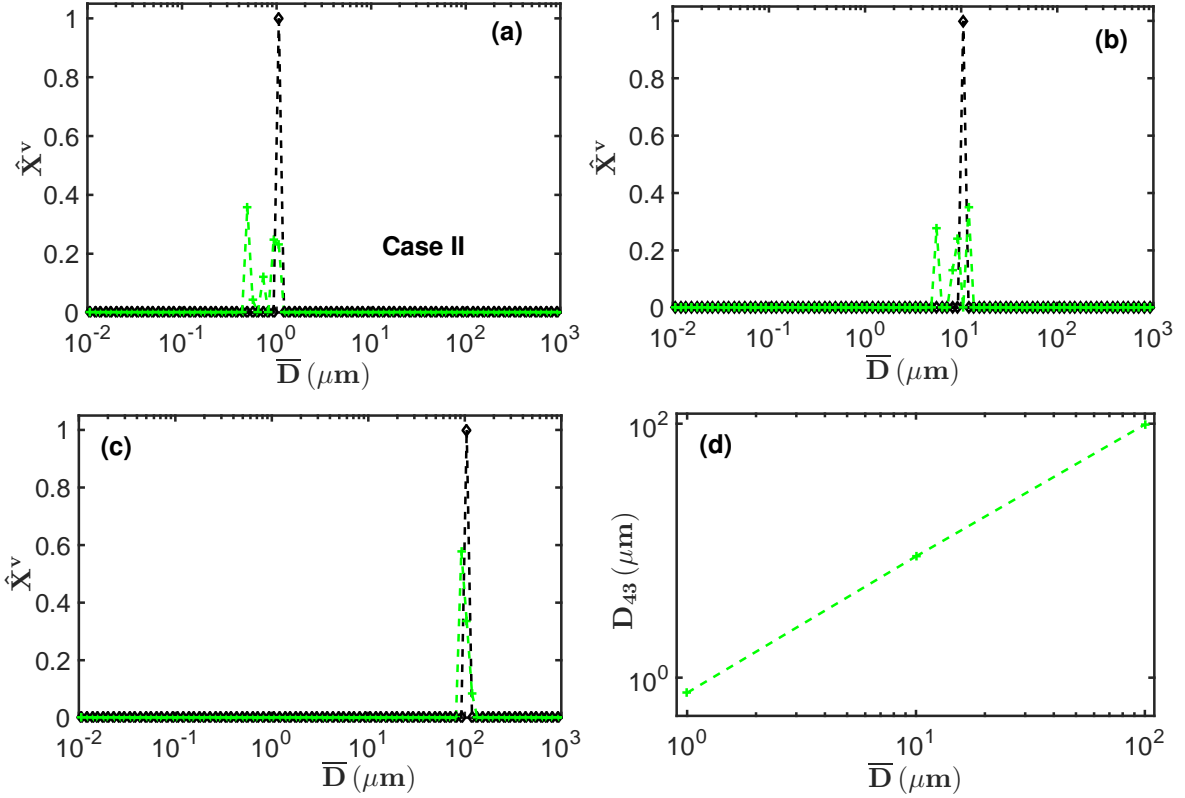


Figure 7: Similar to Fig. 5 but for Case II.

green crosses) at sizes $< 1\mu\text{m}$ in Fig. 7(a) in order to fit the power law regime of the needle-like particles in Fig. 6(a).

As the size of the needle-like particles increases, then the scattering intensity begins to develop strong oscillations, for example the troughs in the black diamonds close to $q = 1\mu\text{m}^{-1}$ and $q = 0.4\mu\text{m}^{-1}$ in Figs. 6(b) and (c) respectively. The oscillations are sufficiently strong such that the scattering intensities of the needle-like particles of sizes $\bar{D} = 10\mu\text{m}$ and $\bar{D} = 100\mu\text{m}$ intersect those of the spherical particles of the corresponding sizes in the power law regime (in Figs. 6(b) and (c)). This is unlike in Case I where the scattering intensities of the needle-like particles of sizes $\bar{D} = 10\mu\text{m}$ and $\bar{D} = 100\mu\text{m}$ (in Figs. 4(b) and (c)) were consistently higher (in the power law regime) than those of spherical particles of corresponding sizes.

The nature of the scattering intensities for these needle-like particles of sizes $\bar{D} = 10\mu\text{m}$ and $\bar{D} = 100\mu\text{m}$ in Figs. 6(b) and (c) causes the spherical model to find a compromise between fitting the troughs and peaks of the oscillations in the scattering intensities for these needle-like particles of sizes $\bar{D} = 10\mu\text{m}$ and $\bar{D} = 100\mu\text{m}$. Hence the fitted curve (green crosses in Figs. 6(b) and (c)) nearly collapses onto the scattering intensities of spherical particles of sizes $\bar{D} = 10\mu\text{m}$ and $\bar{D} = 100\mu\text{m}$ shown by the blue circles in Figs. 6(b) and (c). This compromise situation is also due to the weighting function (Eq. (19)) used in the optimisation. A different weighting function could be

chosen which is optimised for the peaks in the scattering intensities but this will not be the best choice in a general situation.

This compromise situation leads to the prediction of PSDs (green crosses) by the spherical model which contain peaks close to $10\mu\text{m}$ in Fig. 7(b) (for needle-like particles of size $10\mu\text{m}$ shown by the black diamonds) and $100\mu\text{m}$ in Fig. 7(c) (for needle-like particles of size $100\mu\text{m}$ shown by the black diamonds). As the PSDs predicted by the spherical model do not deviate too much from the true PSDs of the needle-like particles in this case, then the estimated D_{43} values by the spherical model also show less deviation from the sizes of the needle-like particles as shown in Fig. 7(d). However, this is just because the spherical model could not find a good fit to the power law regime of the scattering intensities of needle-like particles in this case.

6. Conclusions

We have demonstrated some of the undesired effects of applying a model for scattering by spherical particles to solve the inverse problem for laser diffraction when the scattering intensity comes from a population of needle-like particles. As only simulated data has been used in this work, then the deviations of the estimated PSDs with the spherical model from the PSDs of the needle-like particles are solely the result of using an inappropriate model to fit the data from the needle-like particles.

We have used monodispersed population of needle-like particles in this work to simplify the analysis. However, the spherical model predicts a polydispersed distribution of particle sizes even though the needle-like particles have a monodispersed distribution of sizes. This is because the spherical model tries to fit the scattering intensity as best as it can. Unfortunately, this is the situation with real experimental data. As the PSD is not known, and the inverse problem is not well posed, then a PSD which gives a good fit to the experimental data is chosen as a possible candidate for the true PSD of the population of particles.

This approach is used in commercial laser diffraction instruments, and it can lead to misleading estimates of the PSD of the population of particles under analysis. This is exemplified by the solutions obtained in Case II where the poorer fits to the needle-like particles yielded PSDs which were closer to the true PSDs. However, with real experimental data, these solutions could have been rejected. The estimated PSDs where which yielded better fits to the scattering intensities of the needle-like particles could have been considered more favourably. This approach of relying solely on the goodness of fit of the estimated scattering intensity to the experimentally measured scattering intensity (even though the underlying model for the scattering intensity may not be appropriate) could lead to a gross under estimation of the mean particle size as exemplified by Case I where the estimated D_{43} value for the needle-like particles of size $\bar{D} = 10\mu\text{m}$ was more than 50% less than this value. Therefore, the best way to reduce the risk of predicting misleading PSDs is to apply models that describe the shape of the particles as closely as possible.

Acknowledgement

This work was performed within the UK EPSRC funded project (EP/K014250/1) 'Intelligent Decision Support and Control Technologies for Continuous Manufacturing and Crystallisation of Pharmaceuticals and Fine Chemicals' (ICT-CMAC). The authors would like to acknowledge financial support from EPSRC, AstraZeneca and GSK. The authors are also grateful for useful discussions with industrial partners from AstraZeneca, GSK, Mettler-Toledo, Perceptive Engineering and Process Systems Enterprise. The authors also wish to thank Thomas McGlone and Vaclav Svoboda for providing the images in Fig.1.

References

- [1] C. Washington, Particle size analysis in pharmaceutics and other industries, Ellis Horwood Limited, Chichester, England, 1992.
- [2] D. L. Black, M. Q. McQuay, M. P. Bonin, Laser-based techniques for particle-size measurement: a review of sizing methods and their industrial applications, *Prog. Energy Combust. Sci.* 22 (1996) 267–306.
- [3] C. F. Bohren, D. R. Huffman, Absorption and scattering of light by small particles, John Wiley and Sons, Inc., New Jersey, United States, 1983.
- [4] P. Hamilton, D. Littlejohn, A. Nordon, J. Sefcik, P. Slavin, Validity of particle size analysis techniques for measurement of the attrition that occurs during vacuum agitated powder drying of needle-shaped particles, *Analyst* 137 (2012) 118–125.
- [5] C. Polakowski, A. Sochan, A. Bieganowski, M. Ryżak, R. Földényi, J. Tóth, Influence of the sand particle shape on particle size distribution measured by laser diffraction method, *International Agrophysics* 28 (2014) 195–200.
- [6] E. Lee, L. Pilon, Absorption and scattering by long and randomly oriented linear chains of spheres, *Journal of the Optical Society of America A* 30 (2013) 1892–1900.
- [7] N. C. Wickramasinghe, Light scattering functions for small particles with applications in astronomy, Adam Hilger Ltd., London, United Kingdom, 1973.
- [8] O. S. Agimelen, P. Hamilton, I. Haley, A. Nordon, M. Vasile, J. Sefcik, A. J. Mulholland, Estimation of particle size distribution and aspect ratio of non-spherical particles from chord length distribution, *Chemical Engineering Science* 123 (2015) 629–640.
- [9] O. S. Agimelen, A. Jawor-Baczynska, J. McGinty, J. Dziewierz, C. Tachtatzis, A. Cleary, I. Haley, C. Michie, I. Andonovic, J. Sefcik, A. J. Mulholland, Integration of in situ imaging and chord length distribution measurements for estimation of particle size and shape, *Chemical Engineering Science* 144 (2016) 87–100.

- [10] C. M. Sorensen, Light scattering by fractal aggregates: A review, *Aerosol Science and Technology* 35 (2) (2001) 648–687.
- [11] M. I. Mishchenko, J. W. Hovenier, L. D. Travis, Concepts, terms, notation, in: M. I. Mishchenko, J. W. Hovenier, L. D. Travis (Eds.), *Light scattering by nonspherical particles: theory, measurements and applications*, Academic Press, London, United Kingdom, 2000, Ch. 1, pp. 1–28.
- [12] C. Maetzler, the Matlab code developed by Christian Maetzler for computing the scattering coefficients based on the Mie model can be found in: <http://omlc.org/software/mie/>. Accessed on 23 February 2016.
- [13] S. Boyd, L. Vandenberghe, *Convex optimization*, Cambridge University Press, Cambridge, UK, 2004.
- [14] M. Schenk, A. Thumann, T. Seeger, A. Leipertz, Pure rotational coherent anti-Stokes Raman scattering: comparison of evaluation techniques for determining single-shot simultaneous temperature and relative N₂-O₂ concentration, *Applied Optics* 37 (24) (1998) 5659–5671.
- [15] R. C. Aster, B. Borchers, C. H. Thurber, *Parameter estimation and inverse problems*, Elsevier Inc., Amsterdam, Netherlands, 2013.
- [16] H. G. Merkus, *Particle size measurements fundamentals, practice, quality*, Springer Science & Business Media B.V., Netherlands, 2009.
- [17] M. I. Corp., A primer on particle sizing by static laser light scattering, http://www.particletesting.com/Repository/Files/A_Primer_on_Particle_Sizing_by_Static_Laser_Light_Scattering.pdf, accessed on 23 February 2016 (January 2000).